PAPER

Characterization of polymer-based piezoelectric micromachined ultrasound transducers for short-range gesture recognition applications

View the article online for updates and enhancements.

IOP ebooks™

Bringing you innovative digital publishing with leading voices to create your essential collection of books in STEM research.

Start exploring the collection - download the first chapter of every title for free.

Characterization of polymer-based piezoelectric micromachined ultrasound transducers for short-range gesture recognition applications

Pieter Gijsenbergh[ID]**, Alexandre Halbach, Yongbin Jeong, Guilherme Brondani Torri, Margo Billen, Libertario Demi, Chih-Hsien Huang, David Cheyns, Xavier Rottenberg and Veronique Rochus**

IMEC, Kapeldreef 75, 3001 Heverlee, Belgium

E-mail: Pieter.Gijsenbergh@imec.be

Abstract

This paper deals with the design, simulation and characterization of polymer-based piezoelectric micromachined ultrasound transducers (PMUT) (arrays) intended for short-range gesture recognition applications. The presented process flow is fully compatible with existing flat-panel display fabrication. Finite element models were developed for the evaluation of the frequency response, deflection and acoustic pressure output of single PMUT as a function of the membrane diameter. A laser Doppler vibrometer was used to measure the frequency response, membrane velocity and displacement, as well as mode shapes of the microfabricated PMUT in air. An optical microphone was used to measure the pressure emitted by a single PMUT at various distances along the normal axis of the oscillating membrane. A strong correlation between simulations and measurement results is shown. The device geometries most suitable for short-range gesture recognition purposes are selected and the radiation pattern of square arrays is analyzed using simulations. The resonance properties of single PMUT in an array are determined using measurements. An optimized array is used to demonstrate pulse-echo measurements, and the requirements for a simple gesture recognition platform are elucidated.

Keywords: PMUT, PVDF, frequency response, pressure, finite element simulation, laser Doppler vibrometer, gesture recognition

(Some figures may appear in colour only in the online journal)

1. Introduction

In recent years, piezoelectric micromachined ultrasound transducers (PMUT) have shown their capability to be used for high density, cost-effective, and reliable 2D ultrasound transducer arrays compared to traditional piezoelectric ultrasound transducers, which mainly operate in thickness mode [1].

The working mechanism of a PMUT is illustrated in figure 1. In transmission mode, an applied AC signal induces a mechanical strain in the piezoelectric layer sandwiched between the two electrodes. The resulting stress gradient causes the supporting membrane suspended over a cavity to deflect. The thickness of the layers and size of the cavity can be used to modulate the PMUT resonance frequency. Conversely, in reception mode, incoming acoustic waves generate a voltage across the bending membrane.

Although the output pressure is not currently comparable with capacitive micromachined ultrasound transducers (CMUT) [2, 3], the PMUT technology does not require a high DC bias voltage and is thus a better candidate for acoustic transceivers
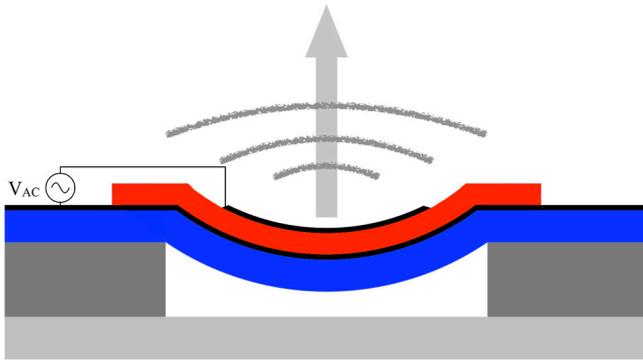
Figure 1. Simplified representation of a PMUT (not to scale). In transmission, the locally actuated piezoelectric layer (red) deflects the membrane (blue), thereby emitting a pressure wave. In receiving mode, an incident pressure wave deflects the membrane resulting in a voltage across the electrodes.

intended for consumer electronics. Moreover, CMUT require a small, well-defined cavity gap in order to achieve a good coupling coefficient, which can be challenging to process. PMUT are significantly less sensitive to the cavity gap size. Lastly, CMUT also tend to suffer from charging effects, whereby electrons are trapped in the dielectric layer and create a drift in performance.

In this paper, we present a novel polymer PMUT design which is compatible with flat-panel display processing. This will allow placing the PMUT arrays close to the display, improving the transmission efficiency and receiving sensitivity. The presented PMUT design is expected to find its ideal implementation in novel acoustic-based applications for electronic devices with flat-panel displays such as haptic feedback [4], fingerprint imaging [5, 6] and gesture recognition. The latter is the driving force behind this article. Thanks to its flexibility in terms of size and acoustic properties, the proposed PMUT design can easily be arranged in a platform of three or four arrays with a quasi-spherical radiation pattern, capable of detecting simple gestures (e.g. push, pull, left, right, clockwise and counterclockwise rotation) which are sufficient to control the basic functions on a laptop, tablet or mobile phone. In a later stage, more complex matrix arrangements could be considered to enable advanced gesture recognition thanks to a spatial resolution allowing to scan a complete hand.

In the following section, the results of a thorough investigation of the properties of single PMUT are presented, including the determination of the resonance frequencies, the (static and dynamic) membrane deflection, the generated pressure output, and a first estimation of the receiving sensitivity. The section includes both measurement results and data obtained by finite element simulations.

The third section of the paper elaborates on the need for the formation of PMUT arrays to achieve a successful pulse-echo system, after defining some basic constraints such as maximum input voltage and minimum output voltage. The maximum obtainable sensing depth for various array sizes is simulated, and important measurement data concerning the single element resonance in arrays is introduced. An optimized array layout is proposed.
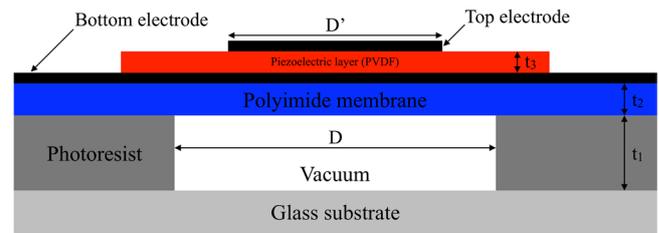

Figure 2. Cross-section of PMUT stack with main parts and geometrical parameters indicated.

The final section presents successful pulse-echo measurements using the optimized array. The requirements to arrange multiple arrays into a full simple gesture recognition platform are clarified, including the main parameters that need to be extracted by the supporting electronics and software.

2. Single PMUT

2.1. Design and fabrication process

The main geometrical parameters for the investigated PMUT structures are indicated in figure 2. The microfabrication process is carried out on a 6-inch glass substrate. Circular microcavities (diameter $D = 200\,\mu m$ to $1000\,\mu m$, $t_1 = 35\,\mu m$) are created using photolithography of a spin-coated negative tone i-line photoresist, which is developed using TMAH. After optimization, the cavity diameter variation across the substrate was reduced to less than $5\,\mu m$. A polyimide membrane ($t_2 = 15\,\mu m$) is suspended above the cavities under low vacuum. Aluminum (~100 nm) is sputtered and subsequently patterned via wet etching to define the bottom electrodes. The actuation layer consists of spin-coated polyvinylidene fluoride (P(VDF-TrFE), $t_3 = 500\,nm$), which is patterned using a chemically amplified i-line photoresist and dry etching. Finally, a second sputter-coated layer of aluminum (~100 nm) is wet etched to define the top electrode of the stack. The diameter ratio of the top and bottom electrode was chosen at $D'/D = 67\%$ in order to achieve the optimal driving efficiency based on prior research [7].

Apart from the metal electrodes, all materials in the current stack are transparent. The transparency and low thermal budget offered by PVDF come at the cost of a lower piezoelectric coefficient, compared to (opaque, high temperature) ceramic such as PZT or BaTiO$_3$ [8, 9]. On the other hand, this polymer-based process flow is entirely compatible with existing flat-panel display fabrication. As such, the PMUT can be produced not only on glass but also flexible substrates, similar to OLED displays. To achieve full display compatibility, a transparent conductor such as indium tin oxide (ITO) can replace the metal electrodes.

2.2. Simulations

A 2D axisymmetric finite element model was implemented in sparselizard [10], an open source multiphysics C + +
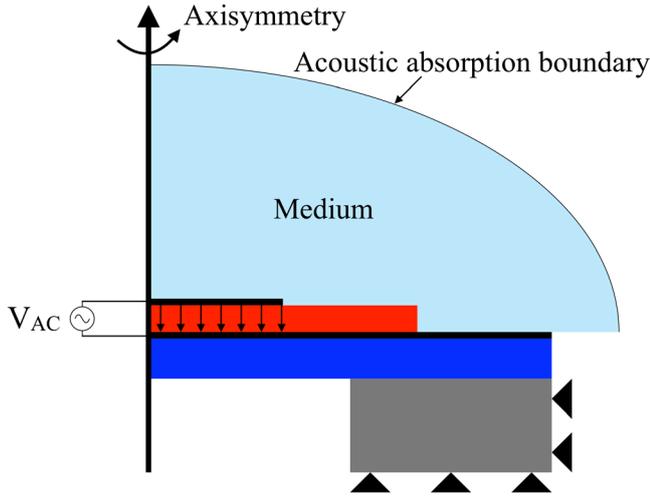
Figure 3. Finite element model overview.

Table 1. Physical properties used in simulations.

Property	Air	Polyimide	Aluminum
Density ρ (kg m^{-3})	1.2	1300	2700
Poisson's ratio ν (—)	—	0.4	0.33
Young's modulus E (GPa)	—	9.75	69
Conductivity σ (S m^{-1})	—	—	3.8×10^7
Relative permittivity ε (—)	1	3	—
Speed of sound c (m s^{-1})	340	—	—

library, using the aforementioned geometrical parameters and the layer stack depicted in figure 2. COMSOL Multiphysics [11] was used to validate all results obtained in sparselizard, although the commercial software package is generally less transparent and limited in use by licensing. The model, illustrated in figure 3, combines a mechanical, acoustical and electrical domain. The external boundaries of the PMUT cavity were mechanically clamped. An acoustic propagation region was created around the device stack to simulate ultrasound waves transmitted or received by the PMUT in a given medium. An absorbing boundary condition was defined to avoid acoustic wave reflections at the edges of the numerical domain. An electric field was applied between the electrodes, across the PVDF layer. An example code for the model shown in figure 3 is also available online [10].

Mechanical, electrical and acoustical properties of the isotropic materials used in the model are summarized in table 1.

Additionally, for the anisotropic PVDF the stiffness matrix required in Hooke's law was defined as

$$
H_{PVDF} = \begin{bmatrix} 3.61 & 1.61 & 1.42 & 0 & 0 & 0 \\ 1.61 & 3.61 & 1.42 & 0 & 0 & 0 \\ 1.42 & 1.42 & 1.62 & 0 & 0 & 0 \\ 0 & 0 & 0 & 0.55 & 0 & 0 \\ 0 & 0 & 0 & 0 & 0.55 & 0 \\ 0 & 0 & 0 & 0 & 0 & 0.69 \end{bmatrix} \text{GPa}
$$

(1)

and the relative permittivity matrix was taken as

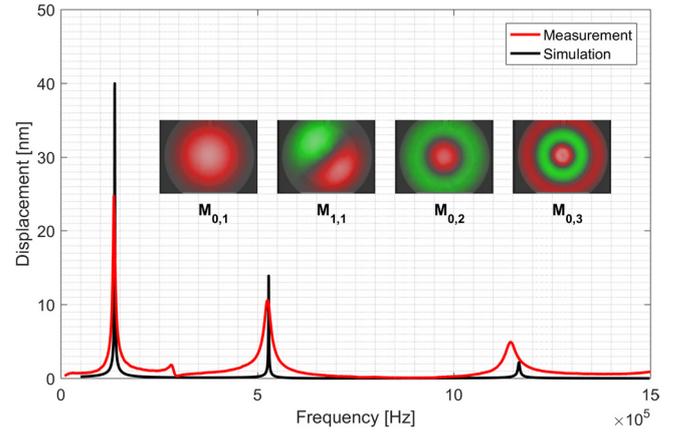**Figure 4.** Measured and simulated frequency response for an 800 μm diameter PMUT. Surface scans in the first three symmetric modes and the first asymmetric mode, corresponding to the peaks in the spectrum are also shown.

$$
\varepsilon_{PVDF} = \begin{bmatrix} 8.1 & 0 & 0 \\ 0 & 8.1 & 0 \\ 0 & 0 & 8.1 \end{bmatrix}
$$

(2)

with a loss tangent equal to 0.12. The density of PVDF was assumed to be 1780 kg m^{-3}.

Linear elasticity equations govern the mechanical domain. The piezoelectric behavior is modeled with classical piezo-electric-elastic coupling equations [12]. From an electrical point of view the electrostatic model is used, and for the acoustic part a linear acoustic model is considered with a Sommerfeld radiation condition [13] on the external face.

The 2D model was first used to determine the resonance frequencies for PMUT membranes with diameters ranging from 200 to 1000 μm. In the mechanical membrane displacement spectrum, resonance manifests as peaks. Additionally, the deflection of the center of the membrane was simulated under a 1 V amplitude sine wave actuation at the first mode resonance frequency. The displacement d of the membrane is related to its velocity v by the vibration/resonance frequency f_r:

$$
v = 2\pi f_r d.
$$

(3)

The pressure and pressure transmission efficiency were simulated in order to enable deducing the maximum achievable depth for successful pulse-echo detection.

To analytically derive the pressure P generated by the oscillating membrane at a given point, the Rayleigh integral [14] can be used, as given by equation (4).

$$
P = \rho f_r \iint_S \frac{v}{R} \alpha e^{-jkR} dS.
$$

(4)

Aside from the density ρ of the medium through which the acoustic waves propagate and the resonance frequency f_r, the velocity v of each point of the membrane surface S is required. These characteristics can be deduced from the peak velocity and the mode shape. Moreover, the distance R between each surface element and the point of interest is required, along
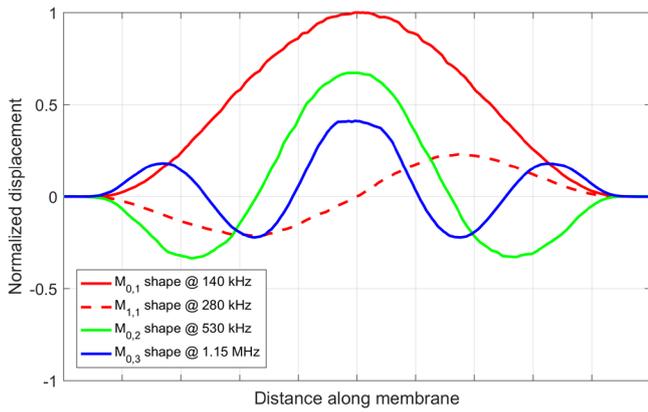
Figure 5. Normalized mode shapes of a single 800 μm diameter PMUT, extracted from the membrane surface scans.

Figure 6. Impedance measurement of a single 600 μm diameter PMUT. The resonance frequency is revealed by a peak in the phase and a change of slope in the impedance.

with a scalar α denoting the attenuation [14] and the wave number k, which is equal to 2π divided by the wavelength.

In addition, a 3D PMUT model was constructed. In this 3D model, the piezoelectric and elasticity equations were solved along with electrodynamic equations. The conduction current is modeled in the aluminum, while the displacement current is modeled in the dielectrics:

$$\text{div}\left(\sigma \text{grad}\left(V\right)\right) = 0 \tag{5}$$

$$\text{div}\left(\varepsilon \frac{\partial}{\partial t} \text{grad}\left(V\right)\right) = 0 \tag{6}$$

wherein V is the electric potential field and the electric field $E = -\text{grad}(V)$. Pressure-induced mechanical stresses act as a source for the electric potential field in equation (6) through piezoelectric coupling. For a given incident pressure, the receiving properties are simulated by attaching an RC load to the PMUT electrodes. An output voltage will be generated across the load, while the output current is given by the integral of the conduction current density flowing through the metal contacts. Conversely, by applying a potential difference across the electrodes and analyzing the in-phase and quadrature currents flowing into the PMUT, its impedance can be derived as a function of the frequency. PMUT resonance appears as peaks in the phase angle, at the same frequencies as in the membrane displacement spectrum.

2.3. Measurement results

Single PMUT were characterized using a Polytec MSA-500 laser Doppler vibrometer (LDV). In a first type of measurement, the bottom electrode of a PMUT was connected to ground while the top electrode was subjected to an actuation signal. A sinusoidal voltage sweep (1 V amplitude, verified by an oscilloscope connected in parallel with the PMUT under test) was applied between 10 kHz and 1.5 MHz. The membrane deflection was measured by focusing the laser on the center of the membrane during the actuation. Figure 4 shows the result of such a measurement on a single 800 μm diameter PMUT, as well as the simulated frequency response.
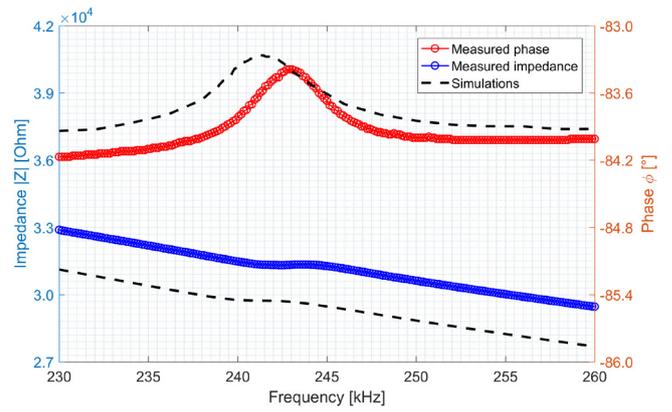
The measured and simulated symmetric mode frequencies correlate well, although the peak deflection is slightly different due to processing and device variations and the fact that simulations did not include any mechanical losses[1]. Moreover, the measurement also appears to reveal a hint of the first asymmetric vibration mode, which is likely due to a small misalignment of the laser or processing defects. Figure 4 also includes the results of detailed surface scans of the PMUT when actuated at each individual mode frequency, revealing the peaks and valleys in the membrane by shades of red and green. The cross-sections of these surface scans, i.e. the mode shapes, normalized to the peak deflection of the first symmetric mode, are shown in figure 5. The mode shape of an actuation at 280 kHz proves that this is indeed the first asymmetric mode.

Aside from characterizing the resonance frequency optically by LDV, it can also be done electrically using an impedance measurement, as illustrated by figure 6. The measurement was performed using a Keysight E4980A Precision LCR meter. At the resonance frequency, the phase angle peaks due to an increase in mechanical losses and acoustic power emission. Simultaneously, the slope of the impedance changes. Decomposing the measured values into the resistive and capacitive contributions reveals that the resistance also peaks at resonance, whereas the capacitance drops slightly.

The offset between the phase and the ideal $-90°$ seen in pure capacitors is attributed to the dielectric losses in the PVDF layer [15].

By expanding the measurements to more PMUT and including different diameters, the average resonance frequency can be charted as a function of the membrane diameter, as shown in figure 7 for the first three symmetric modes up to 2 MHz. Between different PMUT of the same size, there is some variation due to processing, but in general the measured values correlate very well with the values extracted from the simulations. Any deviations can be contributed to differences between the model and the actual

---

[1] The lack of mechanical losses in the 2D model results in very narrow resonance peaks. In the 3D model, mechanical losses were included.
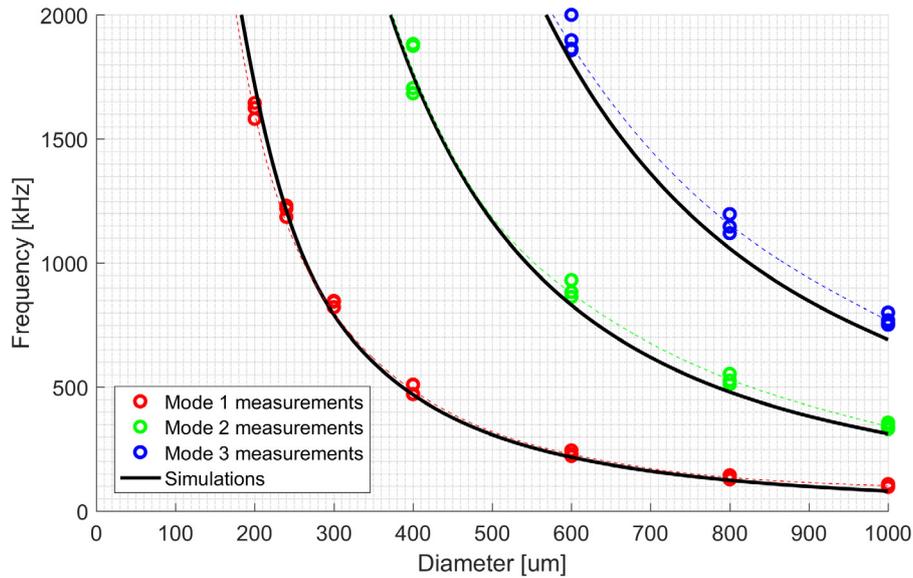
Figure 7. Frequencies for the first three symmetric modes up to 2 MHz for PMUT diameters between 200 and 1000 μm.

devices, including (1) the non-ideal clamping of the membrane edge, and (2) processing-related thickness or stiffness variations.

By driving a PMUT at its (first) resonance frequency using a monochromatic sinusoidal signal, the laser Doppler vibrometer was used to obtain the displacement efficiency as a function of the diameter. Figure 8 shows the measurement results obtained from three sets of PMUT, as well as the simulation results from sparselizard (which were also validated in COMSOL). For diameters up to 600 μm, measurements and simulation agree well, but for larger membranes, the curves tend to diverge.

To gain a better insight into the discrepancy in displacement output, an optical profile meter (Veeco Wyko NT3300) with a custom probe station was used to measure the static deflection when the PMUT were unactuated. These measurements reveal that for large diameter, i.e. above 600 μm, the membranes are no longer flat, as seen in figure 9.

The origin of the static deflections is attributed to two effects. On one hand there is the low vacuum inside the cavity, causing the membrane to be pushed downward by the acting atmospheric pressure above it. Secondly, there is also a bending induced by the internal stress introduced in the electrode metal during sputter deposition [16]. As the finite element models assume a flat, unstressed membrane, the significant static deflection occurring beyond 800 μm may explain the increasing discrepancy between measured and simulated displacement at resonance seen in figure 8.

The displacement efficiency—and hence also the membrane velocity (see equation (3)) and the expected achievable pressure (see equation (4))—trend strongly downward for membrane diameters exceeding 800 μm. As such, the largest PMUT (1000 μm) are no longer considered for the gesture recognition platform.
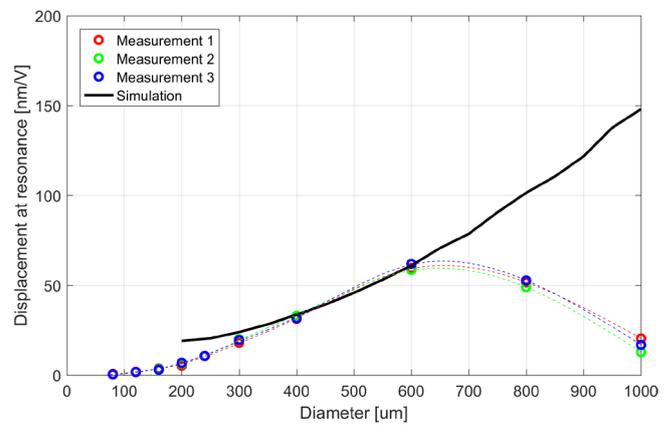

Figure 8. Simulated and measured membrane displacement at the first mode resonance frequency.
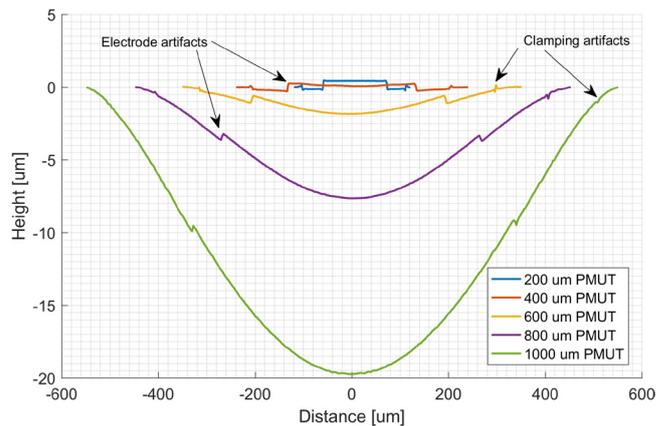

Figure 9. Static deflection of PMUT membranes measured by optical profile meter. The smallest devices are flat whereas the bigger devices have an increasingly deformed membrane. Due to the PVDF transparency, the overlap of the top electrode with the bottom electrode appears as a discrete 500 nm step.

A XARION Eta100 Ultra membrane-free optical microphone [17] was used to measure the pressure emitted by three single PMUT of different size. The microphone was mounted parallel to the glass substrate on an adjustable linear scale, and connected to an oscilloscope. Alignment between the microphone and each PMUT was achieved by peak pressure detection in a horizontal plane above the PMUT. The three PMUT were then each excited by a burst of 40 periods of a sinusoidal signal at their resonance frequency and with an amplitude of 10 V. The time between the actuation of the PMUT and the arrival of the pressure signal at the microphone was used to accurately determine the height of the microphone along the normal axis above the membrane.

The results are graphically represented in figure 10, which also includes a simulation result for an 800 μm diameter PMUT with resonance frequency and deflection value similar to those of the measured PMUT. A reasonable fit between measurement and simulation was obtained and from the simulated curves the pressures at the membrane surface were extracted. These T_x values are 13.8, 12.1 and 8.6 Pa V^{-1} for the 800, 600 and 400 μm devices respectively.

In terms of receiving performance, single PMUT were characterized by actuating them acoustically using off-the-shelf transceivers and measuring the PMUT output voltage using an oscilloscope. Subsequently the pressure output from the transducer was measured using the XARION Eta100 Ultra microphone under the same circumstances. From these measurements, the average reception characteristics were calculated and summarized in table 2.

For an infinite load, an ideal 600 μm diameter PMUT should be able to output approximately 300 μV per Pascal of incident pressure. However, due to the capacitive loading by probes and the coaxial cable (101.05 pF m^{-1}) towards the oscilloscope, this value is significantly reduced. The larger capacitance of larger PMUT should in theory be more capable of driving the finite load, however as their membrane deflection—and as such the strain in the piezoelectric layer—is lower, the increase in measured output voltage is limited. The low internal capacitance and deflection of the 400 μm diameter PMUT result in the lowest measured receiving efficiency. It should be noted that output losses can be significantly reduced by connecting the PMUT directly to integrated read-out electronics.

The suitability of each PMUT for a pulse-echo system is determined not only by the transmit and receive properties, but also by the attenuation of the pressure wave through air. This attenuation increases dramatically with frequency and is also impacted by the temperature and humidity [14]. Table 3 summarizes the resonance frequencies of the PMUT and shows the expected acoustic attenuation at 20 °C and 50% humidity.

Based on the low reception efficiency and large attenuation related to the 400 μm PMUT, they are not further considered for the gesture recognition platform.

2.4. Operation constraints and pressure field

The maximum working depth for a single PMUT of a given size can be calculated by fixing the actuation and detection
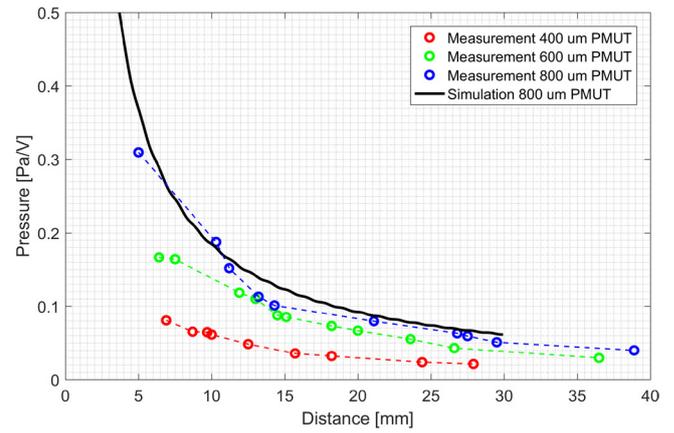

Figure 10. Measured pressure output along the normal axis of different PMUT. The simulated pressure of an 800 μm diameter PMUT is also shown.

Table 2. Measured receiving characteristics.

Diameter (μm)	Measured deflection (nm V^{-1})	Measured R_x (μV Pa^{-1})
400	32	46
600	62	107
800	51	134

Table 3. Resonance frequencies and attenuation coefficients.

Diameter (μm)	Frequency f_{res} (kHz)	Attenuation α (dB m^{-1})
400	490	40.3
600	240	11.1
800	150	5.4

threshold voltages. In transmission, no more than $V_{T, max} = 20$ V$_{ac}$ can be applied to the PMUT, to avoid altering the polarization of the piezoelectric layer. Although applying an additional DC offset signal would allow a higher AC actuation signal, the resulting voltages would soon become difficult to implement in real-life applications. For the receiving mode, $V_{R, min} = 100$ μV is fixed as the minimum requirement. With transmission and reception properties fixed, equation (7) can be used to calculate how much pressure (dB) can be lost along the way towards (and back from) a reflector due to attenuation (see table 3) and geometrical spreading.

$$L_{max} = 20\log_{10}\left[\frac{T_x R_x V_{T,max}}{V_{R,min}}\right]. \tag{7}$$

Assuming a reflection coefficient equal to one, this means the maximum one-way losses allowed for a 600 μm and 800 μm PMUT are 24 dB and 25 dB respectively.

As shown by the simulation results presented in figure 11, the acceptable losses are already reached at 1.7 and 1.9 mm respectively, which is not nearly enough to produce a usable gesture recognition platform. The solution to this is grouping PMUT into arrays to achieve a higher pressure output.

Between acoustic output power and electrical input power, simulations predict an efficiency of approximately 0.5% for each PMUT.
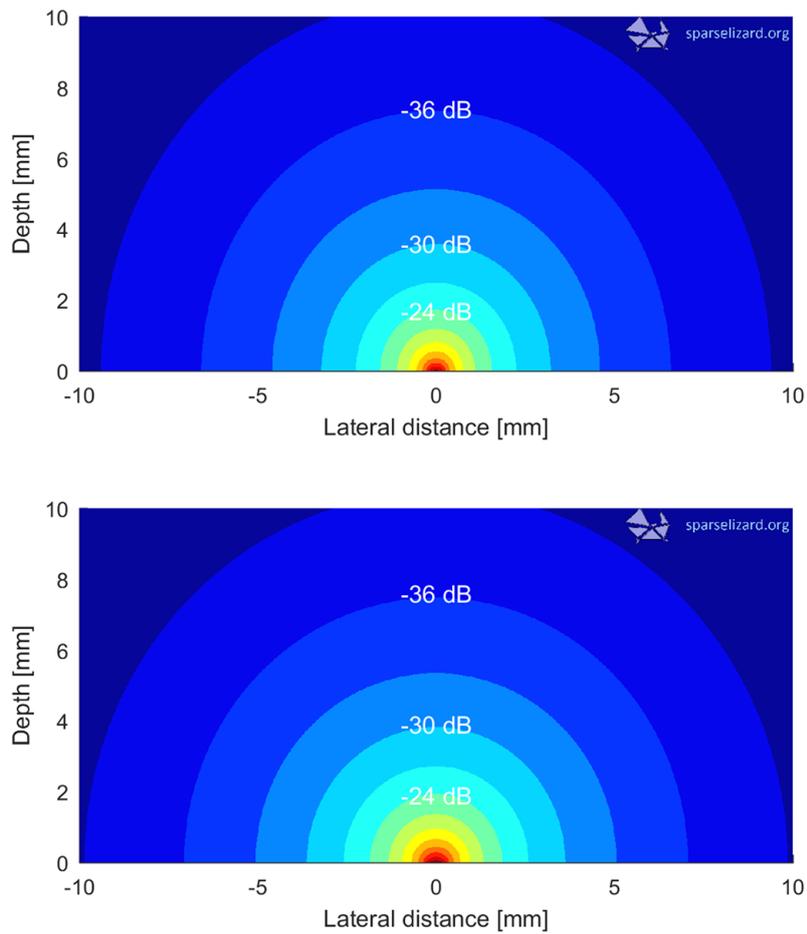
Figure 11. Radiation plot of a single PMUT. Every color level indicates an additional loss of 3 dB. (top) 600 μm diameter. (bottom) 800 μm diameter.
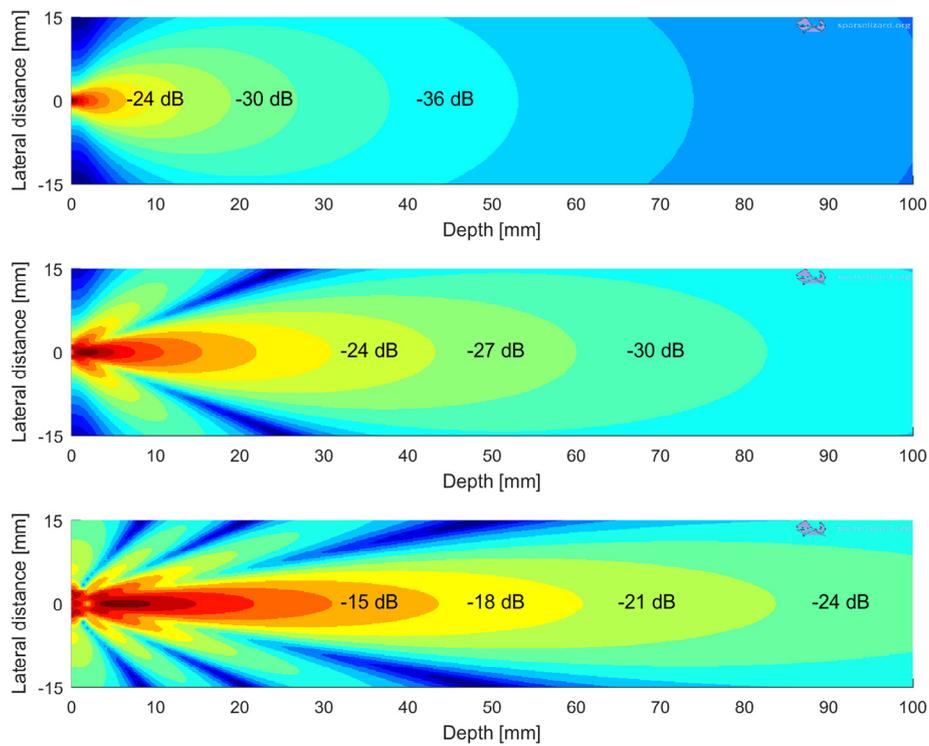

Figure 12. Radiation plots for PMUT arrays. Every color level indicates an additional loss of 3 dB. (top) 2 $\times$ 2 array. (middle) 4 $\times$ 4 array. (bottom) 7 $\times$ 7 array.
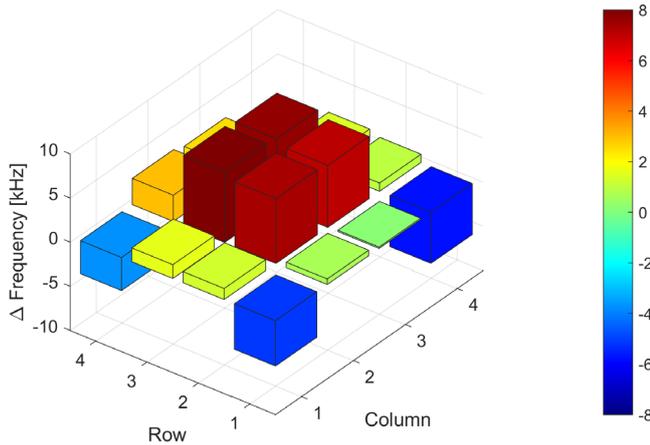
7

Figure 13. Resonance frequency mismatch in 4 × 4 array of 800 μm diameter PMUT.
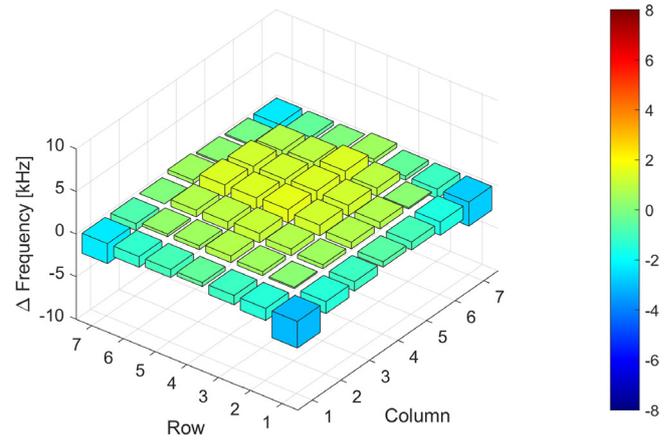
3. PMUT array

3.1. Array requirements and simulations

The circular PMUT presented in the previous section can be organised in (square) arrays to achieve a higher total pressure emission. An important consideration in this matter is the spacing of the PMUT and the total area covered by the array. Ideally, the spherical pressure fields emitted by the single PMUT combine into one main pressure lobe emitted perpendicular to the array plane. To avoid the formation of significant side lobes, the pitch between the elements should be smaller than half the wavelength corresponding to the resonance frequency of the PMUT. On the other hand, a minimum distance between devices is required to guarantee microfabrication reliability. To allocate a 600 μm diameter PMUT, the required area will therefore be approximately 0.49 mm^2, while for an 800 μm device 0.81 mm^2 is needed. As the T_xR_x-product is highest per unit area for the 600 μm PMUT, only these devices will be considered in the following simulations.

Figure 12 shows the simulated radiation pattern for three different square arrays of 600 μm PMUT: 2 × 2, 4 × 4, and 7 × 7. For a simple gesture recognition system, a working depth of 10 cm is a reasonable assumption. Taking into account the calculated allowed losses, it is clear that only the 7 × 7 array (or larger) will satisfy the requirements. Notwithstanding the PMUT pitch was chosen to not exceed half the wavelength, some minor side lobes still tend to appear in the radiation patterns. However, their lateral extension is far smaller than the depth reached by the main lobe and they are as such not considered to be problematic.

3.2. PMUT array measurements

Prototype 4 × 4 arrays of 800 μm diameter PMUT were fabricated on the same substrate as the single PMUT[2] and characterized by LDV to determine the resonance frequency of each element in the array configuration. Figure 13 shows that the operating frequency of the individual devices

[2] The PMUT diameter and number of elements for this prototype array were chosen in the first mask design phase, before any measurement results for the single PMUT were available.
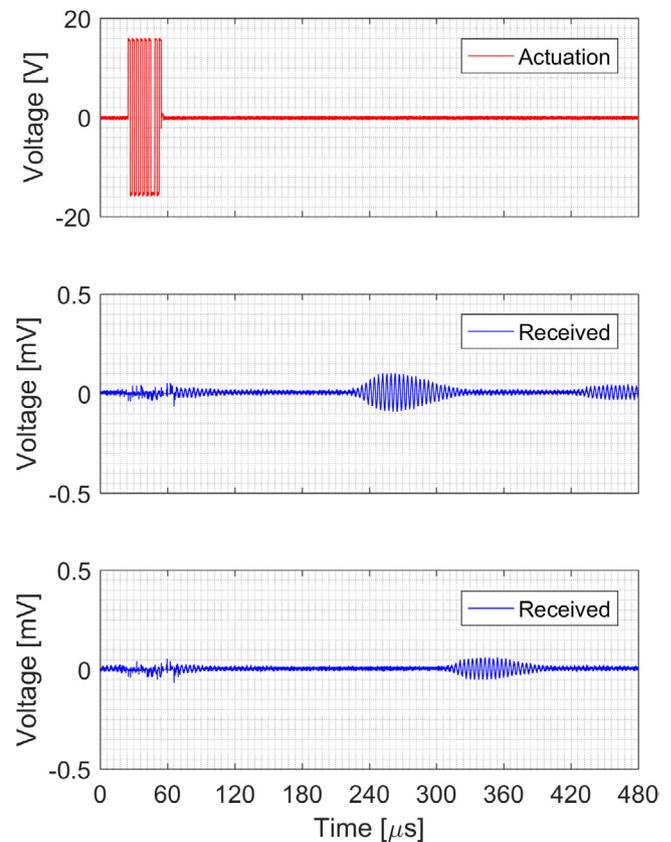

Figure 14. Resonance frequency mismatch in 7 × 7 array of 600 μm diameter PMUT with dummy cavities around.

Figure 15. Pulse-echo measurements. (top) Actuation signal sent to PMUT array. (middle) Received signal with reflector at 36 mm. (bottom) Received signal with reflector at 48 mm.

differs strongly from the optimal array actuation frequency. Moreover, the mutual differences exceed the bandwidth of the PMUT, implying that the full array can never be used at its full potential by applying a single actuation frequency. Based on the pattern observed in figure 13 however, it can be concluded that the resonance frequency of an element is strongly influenced by its surroundings (i.e. corner versus center).

Using these measurement findings as well as the simulation results presented in section 3.1, new 7 × 7 arrays of 600 μm diameter devices were designed and fabricated. To compensate for the resonance frequency offset, two
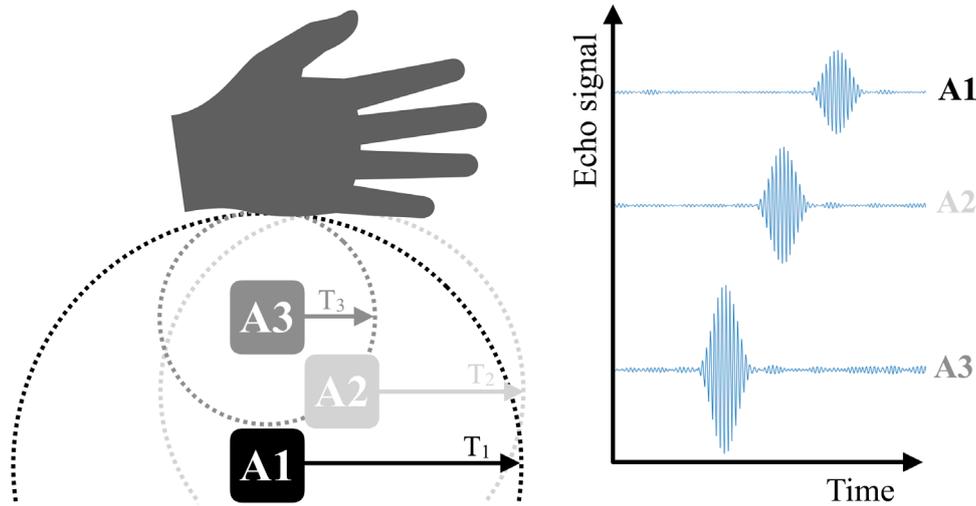
Figure 16. Simple gesture recognition platform using three PMUT array. The pulse-echoes from each array are received with different TOF and amplitude. From changes between consecutive samples, hand motion can be deduced.

rows of dummy elements (i.e. sealed cavities without electrodes) were added around the active array to achieve more uniformity. Figure 14 shows the offset of the individual element resonance frequencies compared to the optimal array driving frequency for the optimized array. The improvement with respect to figure 13 is immediately clear. In this optimized array, all but one PMUT are actuated within their own bandwidth.

4. Gesture recognition platform

Essential to gesture recognition is the acquisition of a pulse-echo signal. To demonstrate that this is possible, the fabricated 7×7 array was connected to a STEVAL-IME011V1 [18] ultrasound pulser evaluation board. A burst of six cycles at the array resonance frequency and with an amplitude of 16 V was applied to the PMUT, before switching into receive mode. A stainless-steel plate serving as a reflector was suspended at various distances above the array. The result of the measurements is shown in figure 15.

In the received signals depicted in figure 15, some interference is visible during the actuation burst. Moreover, when the pulser switches to receive mode, a small voltage resulting from damped motion of the PMUT membranes can be observed. Further along the time axis, the echo signal arrives at a delay corresponding to the reflector distance. When the reflector is placed further away, the echo amplitude decreases.

To construct a platform for simple gesture recognition, more than one array is required. For basic hand movements (e.g. left-right or up-down) three arrays are required while for circular movements a fourth array is required. Each array should have a slightly different operating frequency (at least outside the bandwidth of the other arrays) to ensure it is only responsive to its own echo signals [19, 20]. Alternatively, all arrays may have the same operating frequency if they are actuated in a sequential manner.

To accurately determine the position (and especially the movement) of an object (typically a hand), two parameters can be extracted from the transmitted pulse train and the received echo signal. The first one is the time of flight (TOF), which is defined as the time between the transmission of a pulse (train) from an array and the reception of the echo by the array. The TOF is determined by the speed of sound in the medium and will increase as the reflector moves away from the array (as visible in figure 15). Secondly, the amplitude of the received signal can be used, in which case peak detection in the echo envelope needs to be implemented. If an increase is observed from one sample point to the next, the reflector is approaching the array (as also visible in figure 15).

By combining the TOF and/or echo peak data from the different arrays in the platform and analyzing the differences in values from one instance to the next, the movement of the reflector can be detected, i.e. simple gestures can be recognized.

Figure 16 illustrates how the TOF and amplitude of the echo signals received by each array depend on the position of the hand.

The electronics required to support the platform include a waveform generator and power amplifier on the transmission side, and a low noise amplifier, envelope detector and analog-to-digital converter on the reception side. Software controls the timing and data processing.

For fine gesture recognition, such as the motion of individual fingers, a more delicate approach will be required. A single matrix array consisting of individually addressable PMUT will need to be fabricated so that advanced beam forming [19] can be implemented in order to fully scan the hand.

5. Conclusion

Simulation and measurement results for PVDF-based single PMUT with diameters ranging from 200 to 1000 μm were presented. By combining transmission and reception properties, the optimal size range was refined to 600–800 μm. Radiation patterns showed that single devices can not achieve sufficient depth to construct a gesture recognition.

A minimum required array size was determined via simulations and based on input/output voltage characteristics, minimum operating depth and element pitch requirements. Measurements showed individual array elements can have non-uniform resonance properties depending on their place in the array. An optimized 7×7 array of $600\ \mu m$ diameter PMUT, surrounded by dummy cavities was fabricated. Measurements show an improved resonance frequency matching and pulse-echo was successfully measured.

The working principle for a complete simple gesture recognition platform was briefly explained.

The process flow for the polymer-based PMUT arrays is entirely compatible with existing flat-panel display fabrication, which means they could also be fabricated on flexible substrates. Moreover, the opaque metal contacts can be replaced by ITO to achieve a fully transparent stack.

Acknowledgments

ORCID iDs

Pieter Gijsenbergh ⬤ https://orcid.org/0000-0003-0135-6968

References

[1] Qiu Y, Gigliotti J V, Wallace M, Griggio F, Demore C E M, Cochran S and Trolier-McKinstry S 2015 Piezoelectric micromachined ultrasound transducer (PMUT) arrays for integrated sensing, actuation and imaging *Sensors* **15** 8020–41

[2] Helin P, Czarnecki P, Verbist A, Bryce G, Rottenberg X and Severi S 2012 Poly-SiGe-based CMUT array with high acoustical pressure *IEEE 25th Int. Conf. on Micro Electro Mechanical Systems (MEMS)*

[3] Gerardo C D, Cretu E and Rohling R 2018 Fabrication and testing of polymer-based capacitive micromachined ultrasound transducers for medical imaging *Microsyst. Nanoeng.* **4** 19

[4] Carter T, Seah S A, Long B, Drinkwater B and Subramanian S 2013 UltraHaptics: multi-point mid-air haptic feedback for touch surfaces, UIST pp 505–14

[5] Jeong Y, Huang C-H, Cheyns D, Brondani Torri G, Rottenberg X and Heremans P 2017 PMUT device compatible with large-area display technology *16th Int. Symp. on Electrets*

[6] Tang H, Lu Y, Fung S, Tsai J M, Daneman M, Horsley D A and Boser B E 2015 Pulse-echo ultrasonic fingerprint sensor on a chip *2015 Transducers—2015 18th Int. Conf. on Solid-State Sensors, Actuators and Microsystems (TRANSDUCERS)*

[7] Fox C H J, Chen X and McWilliam S 2007 Analysis of the deflection of a circular plate with an annular piezoelectric actuator *Sens. Actuators* A **133** 180–94

[8] Sadeghpour S and Puers R 2018 Optimization in the design and fabrication of a PZT piezoelectric micromachined ultrasound transducer (PMUT) *Multidisciplinary Digital Publishing Proc.* p 2

[9] Gao J, Xue D, Liu W, Zhou C and Ren X 2017 Recent progress on BaTiO$_3$-based piezoelectric ceramics for actuator applications *Actuators* **6** 24

[10] Halbach A 2017 Sparselizard—the user friendly finite element C + + library (Online: www.sparselizard.org/)

[11] COMSOL Multiphysics (Online: www.comsol.com)

[12] Landis C M 2002 A new finite-element formulation for electromechanical boundary value problems *Int. J. Numer. Methods Eng.* **55** 613–28

[13] Sommerfeld A 1949 *Partial Differential Equations in Physics* (New York: Academic)

[14] Kinsler L E, Frey A R, Coppens A B and Sanders J V 1999 *Fundamentals of Acoustics* 4th edn (New York: Wiley)

[15] Wang S, Liu L, Zeng Y, Zhou B, Teng K, Ma M, Chen L and Xu Z 2015 Improving dielectric properties of poly(vinylidene fluoride) composites: effects of surface functionalization of exfoliated graphene *J. Adhes. Sci. Technol.* **29** 678–90

[16] Gijsenbergh P, Driesen M and Puers R 2011 Controlled stress-induced shaping of molybdenum microstructures *Proc. Eng.* **25** 309–12

[17] Xarion laser acoustics (Online: https://xarion.com/products/eta100-ultra)

[18] STEVAL-IME011V1 Cost effective ultrasound pulser IC evaluation board based on the STHV748 (Online: www.st.com/en/evaluation-tools/steval-ime011v1.html)

[19] Demi L, Viti J and Kusters L 2013 Implementation of parallel transmit beamforming using orthogonal frequency division multiplexing achievable resolution and interbeam interference *IEEE Trans. Ultrason. Ferroelectr. Freq. Control* **60** 2310–20

[20] Demi L, Ramalli A, Giannini G and Mischi M 2015 *In vitro* and *in vivo* tissue harmonic images obtained with parallel transmit beamforming by means of orthogonal frequency division multiplexing *IEEE Trans. Ultrason. Ferroelectr. Freq. Control* **62** 230–5